REPORT DOCUMENTATION PAGE

Form Approved
OMB No. 0704-0188

1. REPORT DATE *(DD-MM-YYYY)*	**2. REPORT TYPE**	**3. DATES COVERED** *(From - To)*
14-10-2011	Journal Article	

4. TITLE AND SUBTITLE

Detectability of Delaminations in Solid Rocket Motors with Embedded Stress Sensors

5a. CONTRACT NUMBER

5b. GRANT NUMBER

5c. PROGRAM ELEMENT NUMBER

6. AUTHOR(S)
Anhduong Q. Le and L.Z. Sun (Univ. of California), and Timothy C. Miller

5d. PROJECT NUMBER

5f. WORK UNIT NUMBER
33SP0769

7. PERFORMING ORGANIZATION NAME(S) AND ADDRESS(ES)

Air Force Research Laboratory (AFMC)
AFRL/RZSM
9 Antares Road
Edwards AFB CA 93524-7401

8. PERFORMING ORGANIZATION REPORT NUMBER

AFRL-RZ-ED-JA-2011-415

9. SPONSORING / MONITORING AGENCY NAME(S) AND ADDRESS(ES)

Air Force Research Laboratory (AFMC)
AFRL/RZS
5 Pollux Drive
Edwards AFB CA 93524-7048

10. SPONSOR/MONITOR'S ACRONYM(S)

11. SPONSOR/MONITOR'S NUMBER(S)
AFRL-RZ-ED-JA-2011-415

12. DISTRIBUTION / AVAILABILITY STATEMENT

Approved for public release; distribution unlimited (PA #11921).

13. SUPPLEMENTARY NOTES
For publication in the Journal of Propulsion and Power.

14. ABSTRACT

A finite element model is used to investigate the effect of delaminations on the radial stress distribution along the bondline during the cooling process of a solid rocket motor composed of propellant, insulation, and casing. With the assumption of stress sensors evenly distributed along the circumference of the interface between the propellant and insulation, a relationship is established between the debond angle, the number of sensors, and the required sensor accuracy. Two approaches are proposed to detect debonds based on the radial stress readings from these embedded sensors. In addition, a quantitative mapping is obtained between the debond size and the sensor data to inversely estimate the extent of the delamination. It is demonstrated that the proposed framework can detect delaminations in solid rocket motors.

15. SUBJECT TERMS

16. SECURITY CLASSIFICATION OF:			**17. LIMITATION OF ABSTRACT**	**18. NUMBER OF PAGES**	**19a. NAME OF RESPONSIBLE PERSON**
					Dr. Timothy C. Miller
a. REPORT	**b. ABSTRACT**	**c. THIS PAGE**	SAR	16	**19b. TELEPHONE NUMBER** *(include area code)*
Unclassified	**Unclassified**	**Unclassified**			N/A

Detectability of Delaminations in Solid Rocket Motors with Embedded Stress Sensors

Anhduong Q. Le[1] and L. Z. Sun[2]
University of California, Irvine, CA 92697-2175

Timothy C. Miller[3]
Air Force Research Laboratory, Edwards AFB, CA 93524

A finite element model is used to investigate the effect of delaminations on the radial stress distribution along the bondline during the cooling process of a solid rocket motor composed of propellant, insulation, and casing. With the assumption of stress sensors evenly distributed along the circumference of the interface between the propellant and insulation, a relationship is established between the debond angle, the number of sensors, and the required sensor accuracy. Two approaches are proposed to detect debonds based on the radial stress readings from these embedded sensors. In addition, a quantitative mapping is obtained between the debond size and the sensor data to inversely estimate the extent of the delamination. It is demonstrated that the proposed framework can detect delaminations in solid rocket motors.

Introduction

Structural health monitoring is of significant interest for the safety and reliability of solid rocket motors (SRMs) [1, 2]. The ability to detect damage in SRMs will help enable timely, accurate, and reliable assessment of structural integrity, and thus will yield great cost savings and prevent catastrophic structural failures [3]. Currently, due to uncertainties associated with service life predictions, many SRMs are disposed of prematurely [4]. A fundamental understanding of thermal-mechanical deformation and related damage mechanisms is critical for the development of improved service life predictions for the next generation of motors.

Because SRMs are cooled from the cure temperature to an ambient temperature, radial stresses persist in the grain throughout its life, and SRMs can develop critical flaws that can cause catastrophic failure at ignition. There

[1] Graduate Student, Department of Civil and Environmental Engineering
[2] Professor, Department of Civil and Environmental Engineering
[3] Materials Research Engineer, Propulsion Materials Applications Branch, Mail Stop RZSM

are three primary failure mechanisms: propellant aging [5-9], bore cracking [10-12], and delamination (debond) at the interfaces between the propellant, insulation, and case [13]. In regions of the grain where a highly triaxial stress state exists, interfacial debond is a predominant damage mode. Little research has focused on using health monitoring to detect this type of defect, although recently Brouwer et al. [13] illustrated the effect of debond on radial stress distributions along the bondline between the propellant and the casing. They employed a two-dimensional linear elastic finite element model to analyze a 20˚ circumferential debond angle at the SRM bondline. While multiple stress sensors [14, 15] were introduced to measure the radial stresses at specific bondline locations, no algorithm was proposed to study the detectability of debonding.

In this paper, we apply the finite element method to investigate the effect of delaminations on the radial stress distribution at the bondline during the cooling process of a solid rocket motor consisting of propellant, insulation, and casing. With the assumption of stress sensors evenly distributed along the circumference of the motor at the propellant/insulation interface, the relationship is established among the debond angle, the number of sensors, and the required sensor accuracy. Two approaches are proposed to detect debonds based on the radial stress readings from the sensors. In addition, a quantitative mapping is obtained between the debond angle and the sensor data to inversely estimate the extent of the delamination. It is demonstrated that the proposed framework can successfully detect delamination damage in solid rocket motors.

Methodology

The solid rocket motor considered is a cylinder with circular cross section as shown in Fig. 1 (symmetry conditions allow only half of the cross section is modeled). The inner and outer grain diameters are 203.2 mm and 406.4 mm, respectively. The thickness of the insulation is 2.54 mm while the casing is 3.175 mm thick. The propellant is a typical composite grain of hydroxyl-terminated polybutadiene/ammonium perchlorate (HTPB/AP). The insulation layer is ethylene propylene diene monomer (EPDM). The temperature-dependent mechanical properties of HTPB/AP and EPDM were obtained from in-house testing at AFRL/RZSM (Edwards AFB). The motor case is assumed to be a filament-wound graphite-epoxy motor (GEM). A simplified symmetric layup with winding angles of $(0^{\circ}/90^{\circ}/\pm45^{\circ})_s$ is assumed and modeled with quasi-isotropic thermal-elastic responses (Young's modulus is 55.9 GPa, Poisson's ratio is 0.30, and the coefficient of thermal expansion is 2.16×10^{-6} K^{-1}) [16].

Most SRMs are designed with stress-relieving slots and flaps or boots near the ends of the grain. Because failure is favored in regions of high stress triaxiality, it is assumed that the propellant/insulation delamination typically

develops first at the motor midplane and propagates longitudinally towards both ends of the motor. The corresponding two-dimensional plane-strain problem can be analyzed using finite element analysis to investigate the effect of debond on the local stress distribution. The analysis is performed using the commercially available finite element software package ABAQUS [17]. Four specific debond cases are considered: the debonds subtend arcs with total angles of 5˚, 10˚, 15˚, and 20˚ (denoted by α in Section A-A of Fig. 1). In some of the figures, the "debond half-angle" is used because of the symmetric finite element model (the debond half-angle is α/2). All cases are subjected to the slow temperature cooling from the cure temperature down to ambient temperature. A stress-free cure temperature of 58˚C is assumed with a final service temperature of -40˚C. An additional 2˚C in temperature drop is used to account for stresses related to cure shrinkage. Therefore, the total effective temperature drop used is 100˚C.

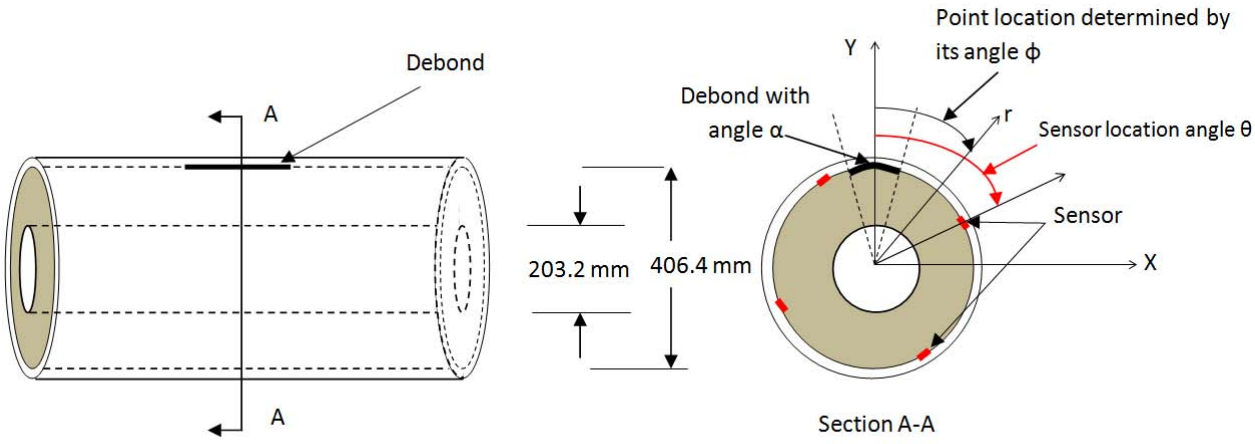

Fig. 1 -- Schematic diagram of a solid rocket motor showing a delamination and an array of four stress and temperature sensors at the midplane of the motor

Plane-strain finite element models of solid rocket motors with debond half-angles of 2.5˚, 5˚, 7.5˚, and 10˚ were analyzed – a typical mesh is shown in Fig. 2, with a debond half-angle of 10˚. The edge of the delamination is modeled as an interfacial crack tip with a heavily refined mesh. Approximately 10390 nodes and 3310 elements were used. The elements were quadratic isoparametric hybrid elements with reduced-order integration (ABAQUS employs hybrid elements, which incorporate pressure as an independent variable, to help prevent computational problems with incompressible or virtually incompressible materials). Symmetry boundary conditions prevent horizontal motion along the left edge, with a single vertical nodal restraint to prevent rigid body motion. The radial, hoop, and shear stresses at the propellant/insulation surface are calculated for temperatures from 60˚C to -40˚C (cooling takes place in a quasistatic fashion with 10˚C increments).

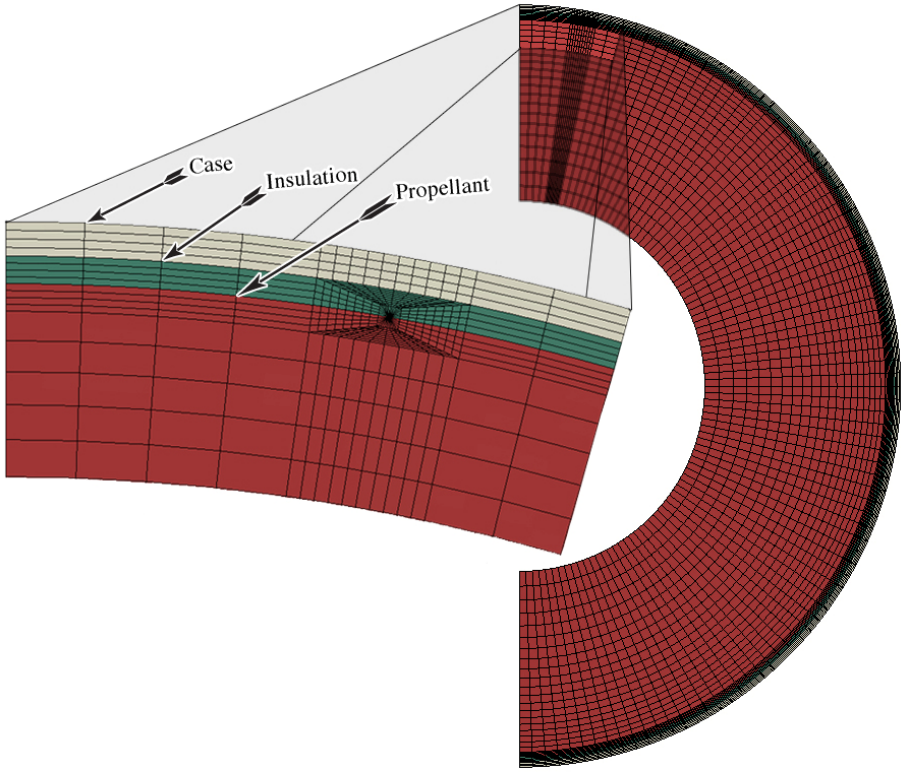

Fig. 2 -- A finite element mesh of the motor midplane. The model shown here has a debond half-angle of 10˚

Results and Discussion

Fig. 3 shows the Dual Bond Stress and Temperature (DBST) sensor that is proposed for health-monitoring of solid rocket motors [14,15]. These sensors have been designed specifically for this purpose, and measure both radial stress (bond stress) and temperature near the case wall. Both wired and wireless prototypes are being developed. Long-term testing and iterative improvements in the manufacturing process have improved accuracy to at least 10 kPa, but significantly greater accuracy is expected due to advances in design and manufacture. Since the sensors measure radial stresses near the case wall, we focused mostly on radial stresses, although hoop stresses are consistently higher in the finite element models (shear stresses are shown in Fig. 4c, however, they are small in comparison to the other two components). In addition, although the presence of a debond clearly perturbs the stresses throughout the entire cross-section of the grain, this work focuses on radial stresses adjacent to the bondline, since these correlate with sensor measurements. Fig. 4 shows typical finite element model contour plots of radial, hoop, and shear stresses (for clarity, the stresses in the propellant only are shown). The plots shown here are for a debond angle of 20˚ at -40˚C.

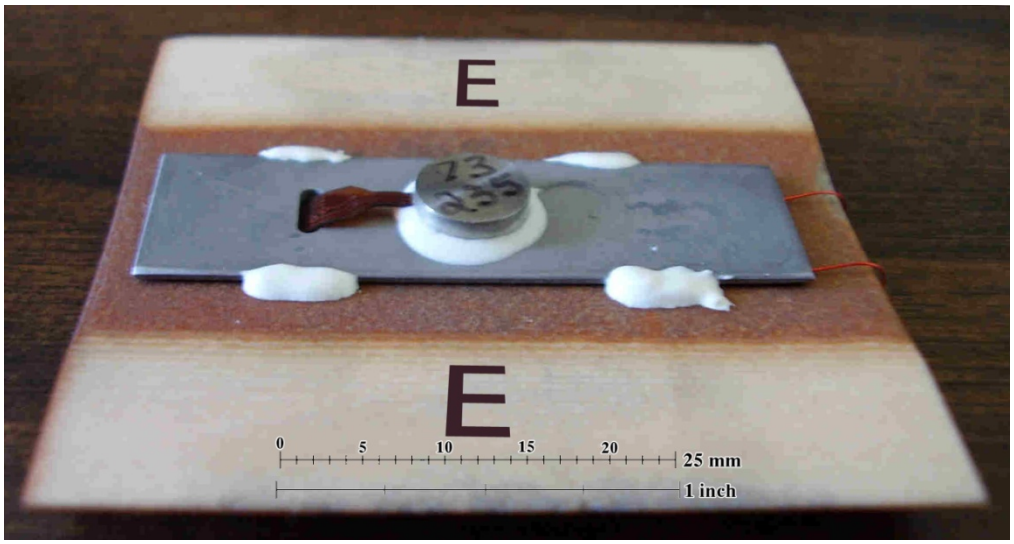

Fig. 3 -- A Dual Bond-Stress and Temperature Sensor mounted on a phenolic case material.

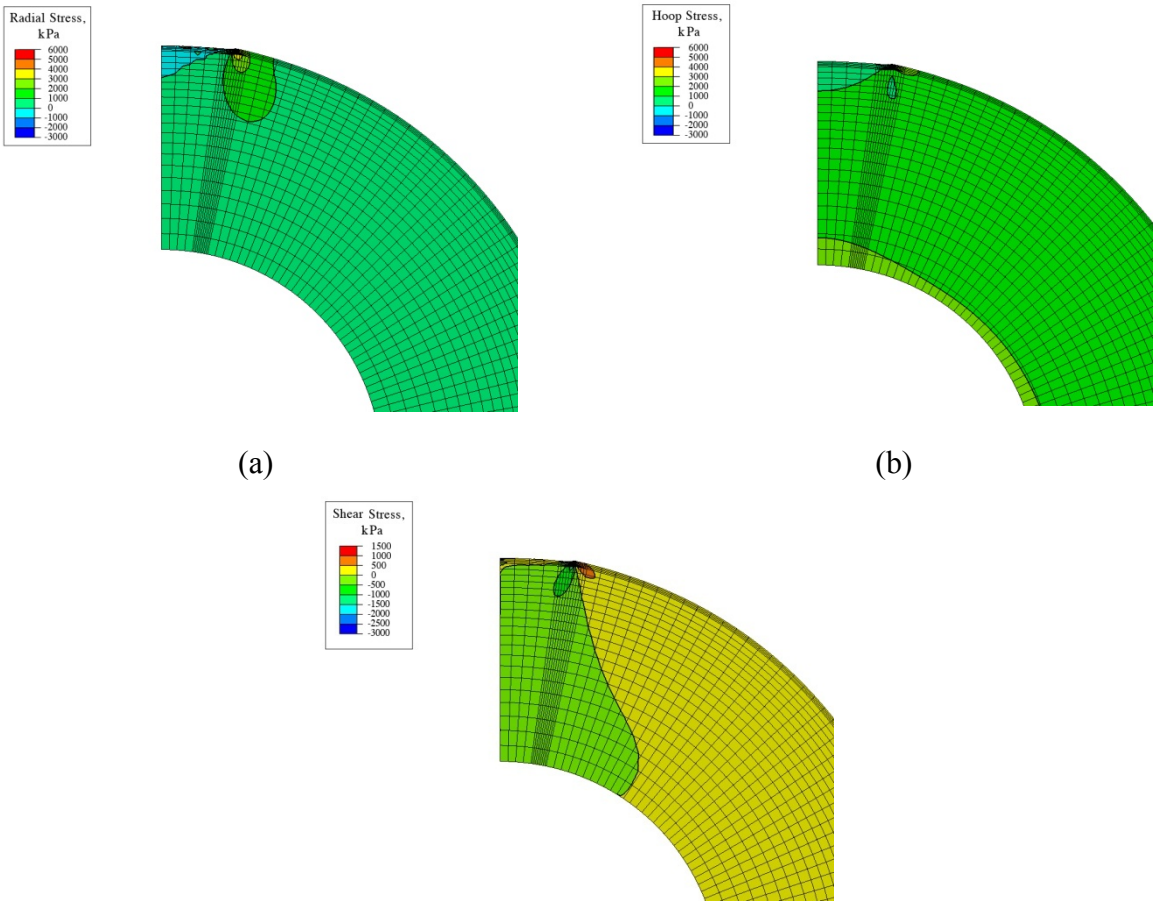

Fig. 4—Distributions of stresses in a motor with a 20˚ debond (a 10˚ debond half-angle) at -40 C

Fig. 5 shows the radial stress distribution over the circumference of the grain of the solid rocket motors in four different debond cases with different debond angles (α = 5˚, 10˚, 15˚, and 20˚). The horizontal line at 855 kPa is the baseline radial stress for a defect-free motor. Obviously, at points remote from the defect, the radial stress approaches its baseline value. At the tip of the debond, the radial stresses exhibit crack-tip like singularities.

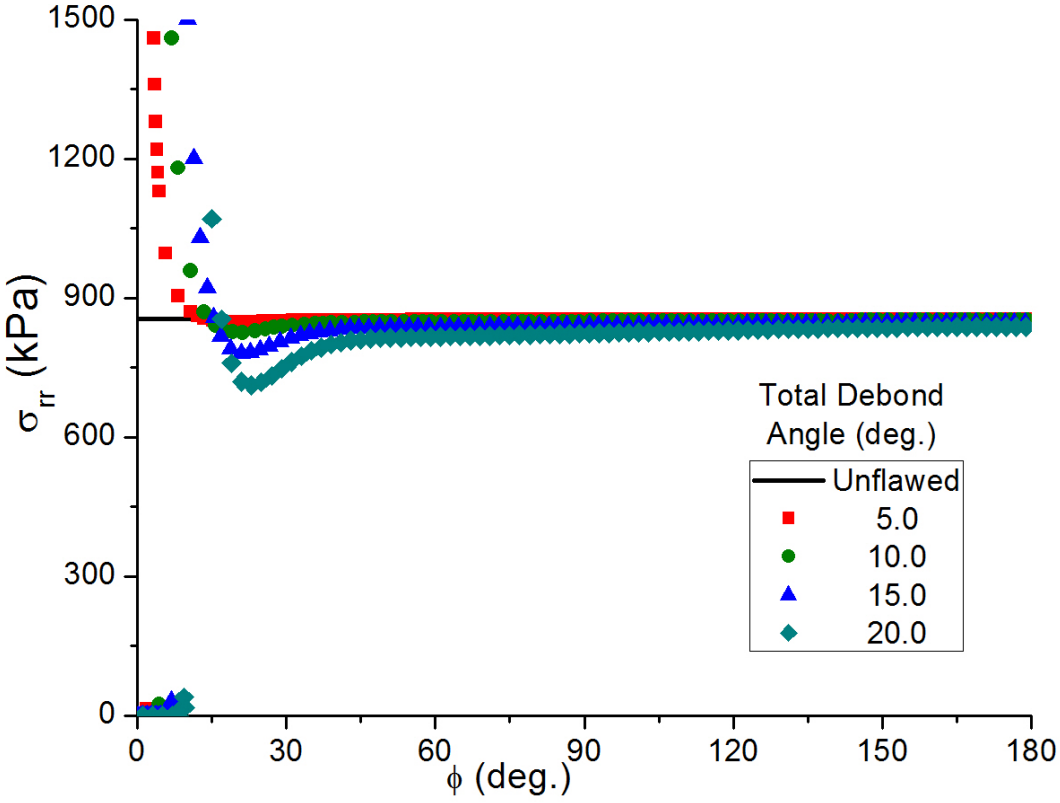

Fig. 5 – Radial stresses along the edge of the propellant grain for various debond sizes (debond angles of 5˚, 10˚, 15˚, and 20˚).

Structural health monitoring can play an important role in detecting rocket motor delaminations. Stress sensors can be embedded at the bondline to measure radial stress around the edge of the propellant grain. Four sensors are first assumed to be evenly mounted with a 90^0 circumferential angle between any two neighbors. Their function is to monitor any possible change of radial stresses. For the detection of debonds, the maximum and minimum values of four sensor readings are compared -- the difference between the highest and lowest radial stresses for various positions of the sensor set is determined (i.e., the position of the sensor set is characterized by θ in Fig. 1). The least optimal location (corresponding to the smallest value of these differences) is compared with sensor accuracy for various defect sizes. In Fig. 6, for example, data for a 20˚ debond angle is shown. The smallest difference between maximum and minimum stress values of the four sensors takes place if θ = 45˚, and this difference is 22.7 kPa. In

other words, no matter where the sensors are located, the difference between the maximum and the minimum values of the four sensor readings is always larger than 22.7 kPa. For the sensors currently being considered, the stress values are accurate to ±10 kPa [14-16]. The implication is that defects with 20˚ debond angles in this solid rocket motor could be detected with 100% reliability.

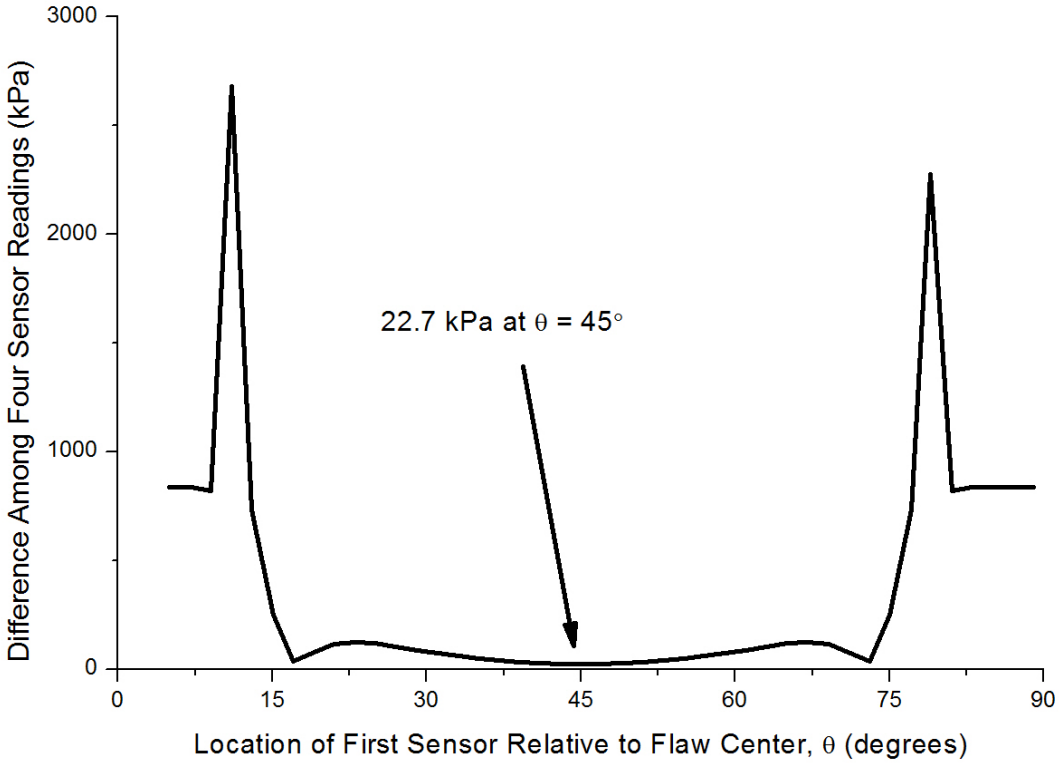

Fig. 6 – Differences among the four stress sensor readings as a function of position. The data shown is for a 20˚ debond angle at the lowest temperature (-40˚C)

Similar analyses were conducted for three-sensor and six-sensor systems. For the 20˚ debond angle, the difference between the maximum and minimum readings at the least-optimal locations were 21.0 kPa and 45.4 kPa respectively. By performing similar analyses (using the finite element models described above) for various debond angles, curves relating the detectable debond angle for three-, four-, and six-sensor systems can be derived and used to construct a set of curves – these results are shown in Fig. 7 below. The figure shows that increasing the number of sensors improves flaw detectability. For example, with six sensors, delaminations with total debond angles at or above 9˚ can be detected with 100% reliability. However, with three- or four sensor- systems, only debonds with angles of at least 15˚ can be detected with 100% reliability.

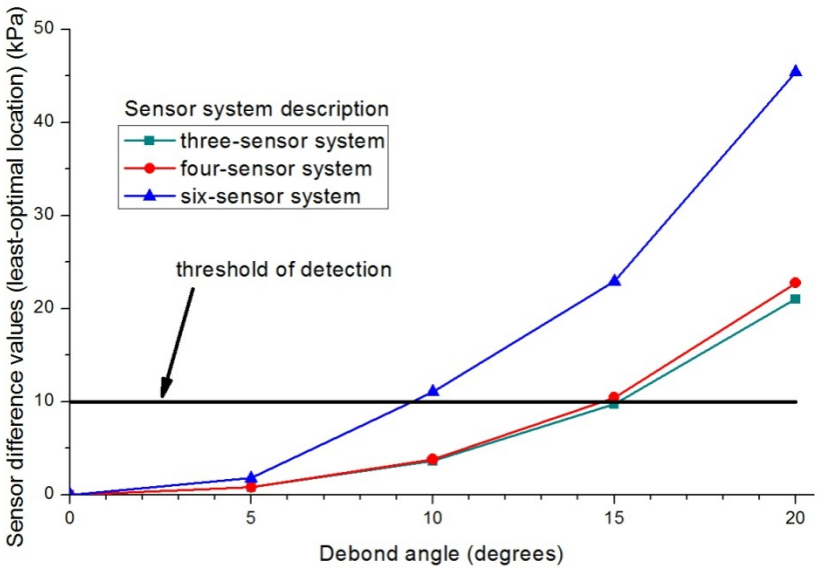

Fig. 7 -- Relationship between stress differences (in the least optimal location) and detectable debond angle using various numbers of sensors

Different temperatures (20˚ C, 0˚ C, - 20˚C and -40˚ C)

Fig. 6 and 7 show results for debonds in a motor at -40˚C, however, these systems will still be able to detect debonds at less extreme temperatures. To examine the effects of temperature on flaw detectability, a four-sensor system is assumed with an initial temperature of 60˚C (the cure temperature is assumed to be 58˚C, however, an additional 2˚C is added to account for curing shrinkage) and final temperatures of 20˚ C, 0˚ C, -20˚C and -40˚ C. The debond angle in this case is 20˚. This part of the analysis is summarized in Fig. 8 below.

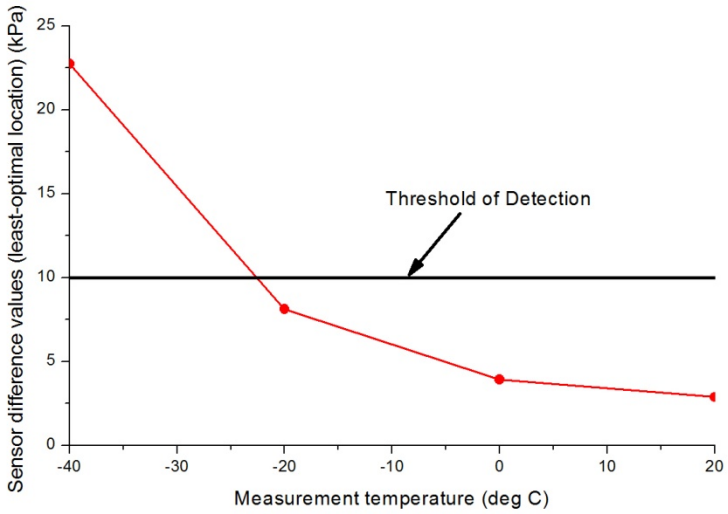

Fig. 8 -- Stress differences in a four-sensor system at the least-optimal location at various temperatures

The figure shows that the detectability is enhanced by taking sensor readings at lower temperatures. For example, by using four sensors, the debond with an angle of 20˚ can be detected with 100% reliability at or below -25˚C. Above this temperature, the probability of detection is less than 100% (but still quite high, as shown later).

As a final comment in this section, the sensitivity of the sensor system to debonds is a function of the sensors themselves, but also the motor geometry and material properties. For the majority of tactical motors, the loading density (or, alternatively, the web fraction) of the propellant would be expected to be higher than in the finite element models employed here – as a result, the work in this paper probably tends to underestimate the sensitivity of the sensors. In this case, more moderate temperatures could probably be employed to sense delamination.

Detectability When One Sensor Fails

The health monitoring system capability is enhanced by using more sensors, and the cost of these sensors is only a fraction of the cost of the motor. However, using an excessive number of sensors can lead to a complicated, expensive system with excessive data storage and analysis requirements. The question arises: what is the best number of sensors to use? Until this point, our discussion has assumed that all sensors in the system work for the duration of the motor life. However, results can be determined if we assume, say, that one of the four sensors in a four-sensor system has failed. It is interesting to note that the debond detectability of the three- and four- sensor systems are very similar. For example, Fig. 7 shows that the difference between stress readings for the three- and four-sensor systems (when the least-optimal location is considered) are 21.0 kPa and 22.7 kPa (assuming a 20˚

debond). On the surface, this suggests that a three-sensor system is ideal, since the results are very close. However, the situation if one sensor is allowed to fail is different. An analysis of the finite element data shows that if this occurs in a four-sensor system, the stress difference (at the least optimal location) between the three remaining sensor readings is 14.4 kPa – so even with one of the four sensors not working, the 20˚ debond can still be detected with 100% probability of detection (assuming 10 kPa sensor accuracy). Figure 9 shows this analysis. Similarly, a three-sensor system was analyzed with a single sensor failure – in this case, the stress difference (at the least optimal location) was less 0.2 kPa (much less than the 10 kPa of sensor accuracy), so having two viable sensors in a three-sensor system is inadequate.

Fig. 9 -- Stress differences for a four-sensor system assuming random failure of a single sensor

A Second Method to Detect Delaminations

In this section, a four-sensor system with a temperature drop from 60˚C to -40˚C is considered. The second method proposed by the authors is to compare sensor readings (at some point during the motor life) with the radial stresses in the flaw-free motor – this method of analyzing the health monitoring data could improve the debond detectability.

The following procedure is proposed. First, use finite elements to determine the radial stresses at the propellant/insulation interface in the flaw-free motor (this is called the “reference value”). Next, determine the largest variation from this reference value for various orientations of the system relative to the flaw. At the least-optimal location, the variation will indicate whether the debond can be detected with 100% reliability. This depends

of course on the sensor accuracy and is a conservative prediction. In the figure below, use of the reference value is referred to as "Method 2" and the method used in the previous section is called "Method 1." The detectability of debonds is increased using Method 2. The only caveat is that any shift in the reference value could affect the viability of the analysis, so if substantial shifts in the stress-free temperature are anticipated, Method 2 must be used with caution.

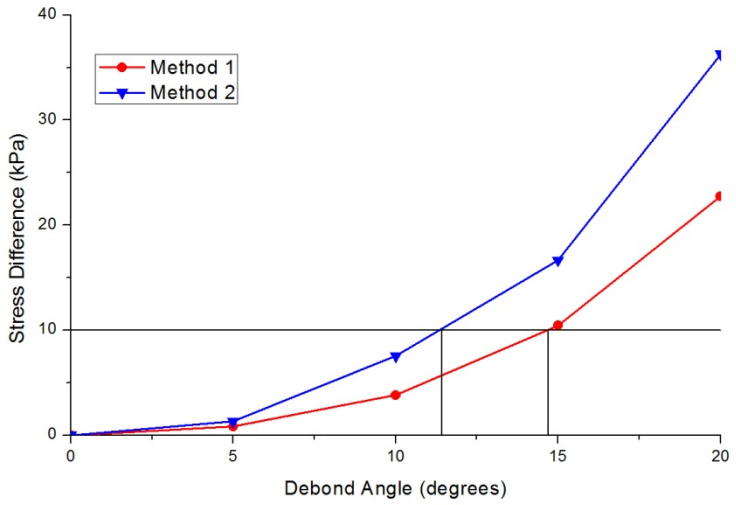

Fig. 10 -- A comparison of flaw detectability using two different methods of detection

Percentage of detectability (reliability)

Previously, we analyzed data in the "least-optimal location," and this gave a conservative estimate of health monitoring system performance. However, this approach ignores most of the data – it is possible to use the entire data set (for example, the curve in Fig. 6, as opposed to its minimum) to determine a probability of detection for a fleet of motors. For any given flaw size, some sensor orientations will have values greater than the sensor accuracy, and some will not. Probability of detection arises from a comparison of such a curve with the sensor accuracy level. In this section, motors with a four-sensor system at -40˚C are analyzed. The following figure illustrates the probability of detection for each debond angle – this again assumes a sensor accuracy of 10 kPa.

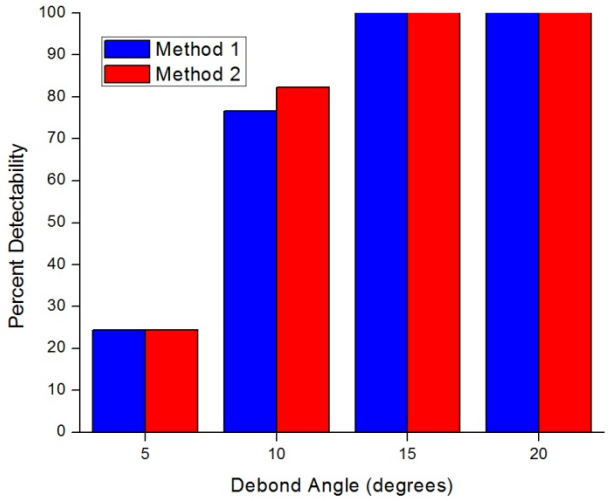

Fig. 11 -- Detectability of flaws for the two proposed methods of analyzing data

Fig. 11 shows that the probability of detection is similar for both methods. Delaminations with debond angles greater than or equal to 15˚ are 100% detectable with either method. Below 15˚, the probability of detection is affected, but is still very high for the 10˚ debond (77% and 82% for Method 1 and Method 2, respectively). Smaller debonds are not very detectable with either method of analysis.

Estimation of debond size (two readings based on medium sensors)

Once the health monitoring data indicates a debond exists, the next question is: how large is the debond? The following method is proposed by the authors to estimate debond angles – in this case, we illustrate it with a four-sensor system and a temperature drop of 100˚C. This method focuses on the absolute difference between the two intermediate values of sensor readings (excluding the maximum and minimum values of sensor readings).

For each location of a set of four sensors, by using the finite element data, the sensors readings are arranged in decreasing order: R_1, R_2, R_3, and R_4. Figure 12 shows the range (scattered points) of value ($R_2 - R_3$) as a function of debond angle. The solid lines in the figure represent the boundaries of maximum and minimum stress values of ($R_2 - R_3$) with all the debond angles considered (0˚ to 20˚). Therefore, at a given debond angle, the values of ($R_2 - R_3$) vary in a defined envelope. With no debond ($\alpha = 0^\circ$ in Fig. 12), R_1, R_2, R_3, and R_4 are always equal, so the stress difference is zero – but this stress difference increases with the size of the debond. To use the graph, the value of ($R_2 - R_3$) is obtained from sensor readings and is referred to the y-component so that the corresponding upper and lower limits for the debond angle (x-components) can be estimated. For example, if the two stress readings R_2 and R_3

differ by 5 kPa, then the corresponding debond is between 11.5˚ and 16.5˚. Similar algorithms may be found for the three- or four-sensor systems to estimate the debond size from the sensor data.

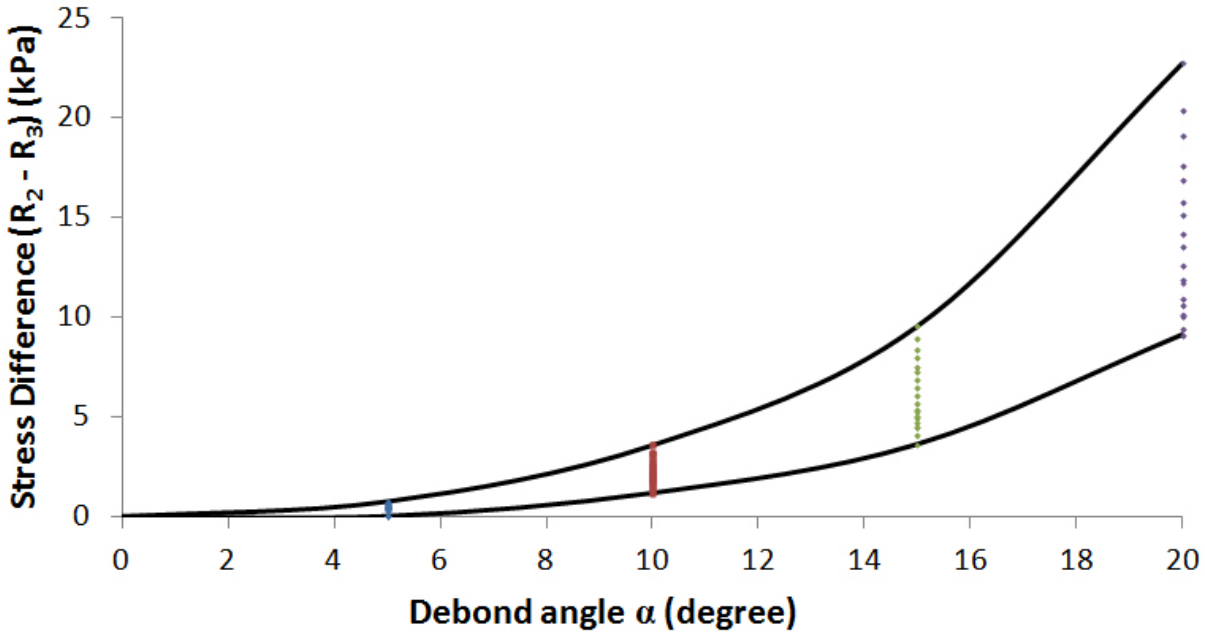

Fig. 12 -- A method for determining the extent of the debond using four-sensor system data

Conclusions

Health monitoring sensor data can be used to detect delaminations (debonds) along the propellant/insulation interface in solid rocket motors. Two methods have been suggested to analyze the data, with similar results. In each case, the sensors measure radial stresses (and temperature) at the interface between the grain and the insulation. The methods are explained and analyzed with finite element models; comparison with sensor manufacturer data indicates that debonds of various sizes can be detected. Furthermore, a quantitative relationship is established that allows estimation of the size of the debond from the sensor data.

Acknowledgements

This work was made possible by the U.S. Air Force Research Lab at Edwards Air Force Base (AFRL), which supported the Air Force Summer Faculty Fellowship Program (SFFP) administered by the American Society for Engineering Education (ASEE). The authors gratefully acknowledge technical assistance from Jim Buswell and Herb Chelner of Micron Instruments in regards to the dual bond stress and temperature (DBST) sensors and Greg Yandek of AFRL/RZSM for the data collection of EPDM insulation material.

References

[1] Ruderman, G.A., "Health management and service life for air force missiles – past and future," *Proceedings of NATO Research and Technology Organization (RTO) Applied Vehicle Technology (AVT) Panel Symposium on Advances in Service Life Determination and Health Monitoring of Munitions (RTO-MP-AVT-176)*, Antalya, Turkey, April 12-15, 2010, pp. 01-1-14.

[2] Little, R.R., Chelner, H., Buswell, H.J., "Development, testing, and application of embedded sensors for solid rocket motor health monitoring," *Proceedings of 37th Annual Conference of Fraunhofer-Institute for Chemical Technology (ICT)*, Karlsruhe, Germany, June 27-30, 2006, pp. 1-12.

[3] Ozupek, S., "Computational procedure for the life assessment of solid rocket motors," *AIAA Journal of Spacecraft and Rockets*, Vol. 47, 2010, pp. 639-648.

[4] Shillig, T.R., Miller, T.C., "Wireless embedded sensors for solid rocket motor health monitoring," *Proceedings of NATO Research and Technology Organization (RTO) Applied Vehicle Technology (AVT) Panel Symposium on Advances in Service Life Determination and Health Monitoring of Munitions (RTO-MP-AVT-176)*, Antalya, Turkey, April 12-15, 2010, pp. 19-1-6.

[5] Judge, M.D., "An investigation of composite propellant accelerated ageing mechanisms and kinetics," *Propellants, Explosives, Pyrotechnics*, Vol. 28, 2003, pp. 114-118.

[6] Iqbal, M.M., Liang, W., "Modeling the moisture effects of solid ingredients on composite propellant properties," *Aerospace Science and Technology*, Vol. 10, 2006, pp. 695-699.

[7] Brouwer, G.C.R., "Ageing of AP/HTPB propellants," *Proceedings of NATO Research and Technology Organization (RTO) Applied Vehicle Technology (AVT) Panel Symposium on Advances in Service Life Determination and Health Monitoring of Munitions (RTO-MP-AVT-176)*, Antalya, Turkey, April 12-15, 2010, pp. 8-1-14.

[8] Brouwer, G.C.R., Buswell, H.J., Chelner, H., "The use of embedded bond stress sensors to determine aging," *Proceedings of 43rd AIAA/ASME/SAE/ASEE Joint Propulsion Conference and Exhibit (AIAA-2007-5788)*, Cincinnati, OH, July 8-11, 2007, pp. 1-11.

[9] Cerri, S., Bohn, M.A., Menke, K., Galfetti, L., "Ageing behaviour of HTPB rocket propellant formulations," *Central European Journal of Energetic Materials*, Vol. 6, 2009, pp. 149-165.

[10] Ho, S.-Y., Care, G., "Modified fracture mechanics approach in structural analysis of solid-rocket motors," *AIAA Journal of Propulsion and Power*, Vol. 14, 1998, pp. 409-415.

[11] Wong, F.C., "Pseudodomain fracture analysis of instrumented analog rocket motors," *AIAA Journal of Spacecraft and Rockets*, Vol. 40, 2003, pp. 92-100.

[12] Tussiwand, G.S., Oley, D., Besser, H.-L., Weterings, F.P., Brouwer, G.C.R., "Application of embedded sensor technology to a full-scale experimental nozzleless rocket motor," *Proceedings of 43rd AIAA/ASME/SAE/ASEE Joint Propulsion Conference and Exhibit (AIAA-2007-5790)*, Cincinnati, OH, July 8-11, 2007, pp. 1-18.

[13] Brouwer, G.C.R., Pfiffer, A., Bancallari, L., "Development and deployment of diagnostic prognostic tactical solid rocket motor demonstrator," *Proceedings of 47th AIAA/ASME/SAE/ASEE Joint Propulsion Conference and Exhibit (AIAA-2011-5788)*, San Diego, CA, July 31-August 3, 2011, pp. 1-11.

[14] Chelner, H., "Embedded sensor technology for solid rocket motor health monitoring," SBIR Phase I Final Report, Contract No. DAAH01-02-R099, U.S. Army Aviation and Missile Command, Redstone Arsenal, Huntsville, Alabama, February 2003.

[15] Buswell, H.J., "Lessons learned from health monitoring of rocket motors," *Proceedings of 41st AIAA/ASME/SAE/ASEE Joint Propulsion Conference and Exhibit (AIAA-2005-4558)*, Tucson, AZ, July 10-13, 2005.

[16] Delmonte, J., *Technology of Carbon and Graphite Fiber Composites*, Van Nostrand Reihold Company, New York, NY, 1981, pp. 198-250.

[17] *ABAQUS Analysis User's Manual, Version 6.6*, ABAQUS, Inc., Providence, RI, 2006.